Mikolaj, M., Reich, M., Güntner, A. (2019): Resolving Geophysical Signals by Terrestrial Gravimetry: A Time Domain Assessment of the Correction-Induced Uncertainty. - *Journal of Geophysical Research*, *124*, 2, pp. 2153—2165.

DOI: http://doi.org/10.1029/2018JB016682

JGR Solid Earth

RESEARCH ARTICLE
10.1029/2018JB016682

Resolving Geophysical Signals by Terrestrial Gravimetry: A Time Domain Assessment of the Correction-Induced Uncertainty

M. Mikolaj[1], M. Reich[1], and A. Güntner[1,2]

[1]Section Hydrology, GFZ German Research Centre for Geosciences, Potsdam, Germany, [2]Institute of Environmental Science and Geography, University of Potsdam, Potsdam, Germany

Key Points:
- Global-scale uncertainty assessment of tidal, oceanic, large-scale hydrological, and atmospheric corrections for terrestrial gravimetry
- Resolving subtle gravity signals in the order of few nanometers per square second is challenged by the statistical uncertainty of correction models
- Uncertainty computed for selected periods varies significantly with latitude and altitude of the gravimeter

Supporting Information:
- Supporting Information S1

Correspondence to:
M. Mikolaj
Email: mikolaj@gfz-potsdam.de

Citation:
Mikolaj, M., Reich, M., & Güntner, A. (2019). Resolving geophysical signals by terrestrial gravimetry: A time domain assessment of the correction-induced uncertainty. *Journal of Geophysical Research: Solid Earth*, *124*, 2153–2165. https://doi.org/10.1029/2018JB016682

Received 11 SEP 2018
Accepted 12 FEB 2019
Accepted article online 14 FEB 2019
Published online 26 FEB 2019

Abstract Terrestrial gravimetry is increasingly used to monitor mass transport processes in geophysics boosted by the ongoing technological development of instruments. Resolving a particular phenomenon of interest, however, requires a set of gravity corrections of which the uncertainties have not been addressed up to now. In this study, we quantify the time domain uncertainty of tide, global atmospheric, large-scale hydrological, and nontidal ocean loading corrections. The uncertainty is assessed by comparing the majority of available global models for a suite of sites worldwide. The average uncertainty expressed as root-mean-square error equals 5.1 nm/s^2, discounting local hydrology or air pressure. The correction-induced uncertainty of gravity changes over various time periods of interest ranges from 0.6 nm/s^2 for hours up to a maximum of 6.7 nm/s^2 for 6 months. The corrections are shown to be significant and should be applied for most geophysical applications of terrestrial gravimetry. From a statistical point of view, however, resolving subtle gravity effects in the order of few nanometers per square second is challenged by the uncertainty of the corrections.

Plain Language Summary Many scientists are exploring ways to benefit from gravity measurements in fields of high societal relevance such as monitoring of volcanoes or measuring the amount of water in underground. Any application of such new methods, however, requires careful preparation of the gravity measurements. The intention of the preparation process is to ensure that the measurements do not contain information about processes that are not of interest. For that reason, the influence of atmosphere, ocean, tides, and hydrology needs to be reduced from the gravity. In this study, we investigate how this reduction process influences the quality of the measurement. We found that the precision degrades especially owing to the hydrology. The ocean plays an important role at sites close to the coast and the atmosphere at sites located in mountains. The overall errors of the reductions may complicate a reliable use of gravity measurements in certain studies focusing on very small signals. Nevertheless, the precision of gravity reductions alone does not obstruct a meaningful use of gravity measurements in most research fields. Details specifying the reduction precision are provided in this study allowing scientist dealing with gravity measurements to decide if their signal of interest can be reliably resolved.

1. Introduction

The high precision of state-of-the-art gravimeters has contributed to their widespread use in geophysics for measuring spatial and temporal variations of gravity of the Earth. The common denominator of studies exploiting terrestrial gravity measurements is the relation of gravity variations to mass transport. Besides the more traditional use of gravimeters in geodesy and geodynamics, for example, to map changes of the Earth's shape (Plag & Pearlman, 2009), in tectonics (Van Camp et al., 2011), or to assess land uplift due to glacial isostatic adjustment (Ophaug et al., 2016; van Dam et al., 2017), terrestrial gravimetry is an emerging monitoring technique in other fields of research. These include monitoring of geothermal fields (Kao et al., 2014), CO_2 storage reservoirs (Sugihara et al., 2017), volcanoes (Carbone et al., 2017; Poland & Carbone, 2016), evapotranspiration rates (Güntner et al., 2017; Van Camp et al., 2016), preseismic and coseismic changes (Imanishi et al., 2004; Vallée et al., 2017), or the definition of the kilogram (Stock, 2013). Many more applications of absolute and relative gravity measurements have been reviewed by Crossley et al. (2013) and Van Camp et al. (2017). Given the ongoing technological advancements in terrestrial gravimetry toward

smaller, more precise, and more affordable instruments, including the development of new technologies such as atom quantum instruments (Gillot et al., 2014; Ménoret et al., 2018) and microelectromechanical devices (Middlemiss et al., 2016), fields of research and application for terrestrial gravimetry can be expected to grow further in the future.

All applications of terrestrial gravimetry share the common challenge of resolving the signal of interest by applying a set of time variable gravity corrections. Taken into account should be all other effects that are part of the integrative gravity measurements due to both mass attraction and Earth's surface deformation. The standard procedure for reducing the observed signal to gravity residuals of interest comprises Earth and ocean tides, variations of the Earth orientation parameters, and atmospheric loading (Hinderer et al., 2015). Especially, if small-scale phenomena are of interest, further corrections for gravity effects of continental (large-scale) hydrology and nontidal ocean loading should be considered. While there are many models available for these processes, there is no recommended procedure in which model should be applied to reduce the gravity observations. This has led to inconsistent approaches among studies so far. For reducing tides, Tanaka et al. (2013), for instance, used the Baytap program (Tamura et al., 1991); other studies preferred ETERNA (Wenzel, 1996), for example, in Meurers et al. (2016), or VAV program (Venedikov et al., 2005), for example, in Arnoso et al. (2011). Much of the same variety can be found even in studies focusing on identical or similar phenomena, like local water storage changes, where for the correction of global atmospheric gravity effects; some studies (Hector et al., 2015) chose the École et Observatoire des Sciences de la Terre (EOST) atmospheric loading (Boy & Hinderer, 2006); and others (Creutzfeldt et al., 2013) preferred Atmacs (Klügel & Wziontek, 2009). Similar examples can by found for continental hydrology and nontidal ocean loading (e.g., Hector et al., 2014; Mikolaj et al., 2015). In view of differences between the various models, it often remains unclear to what extent the result depends on the chosen correction model and whether the signal of interest can be reliably resolved.

The signal of interest can be confidently resolved only if the instrumental precision (or reproducibility), uncorrected ambient and environmental noise, and the uncertainty of applied corrections allow such conclusion from a statistical point of view. The estimation of the instrumental precision requires separation of the noise sources. This can be done by comparing the gravity records of multiple gravimeters operated at the same location. Recently presented results in Rosat and Hinderer (2018) obtained after comparing six superconducting gravimeters (SGs) suggested that the instrumental self-noise can reach 0.003 nm/s^2 in amplitude (or 1 $[nm/s^2]^2/Hz$) power spectral density) at periods between approximately 20 s up to 1 hr. The noise amplitude increases for daily periods approximately by a factor of 10 (100 for power spectral density). In the time domain, the SG precision was in Hinderer et al. (2015) estimated to be 1 nm/s^2 based on a review of several studies comparing colocated and dual-shere SG measurements. The long-term precision of SG records is directly dependent on the reproducibility of FG5 absolute gravimeters used to correct the instrumental drift of SGs. The long-term reproducibility of FG5 absolute gravimeters was estimated in Van Camp et al. (2005) to be at the level of 16 nm/s^2. The aforementioned values do not take systematic effects or the uncertainty of gravity corrections into account.

The aim of this study is to quantify the uncertainty of selected gravity corrections. The uncertainty is assessed comparing commonly applied correction models. The acquired differences are in accordance with Joint Committee for Guides in Metrology (2008) used to compute the root-mean-square error (RMSE) characterizing the dispersion of correction models. The results reveal to which extent the correction procedure contributes to the overall uncertainty of gravity residuals and which are the main components affecting the resulting uncertainty. For the correction procedure, we follow an average user's perspective who selects one or another correction model without prior knowledge of the true and actually unknown value. We consider only those corrections for which a variety of basically indistinguishable models is available, that is, where a regular user cannot infer a preference for a distinct model from literature. This limits the range of examined corrections to global atmospheric, tidal and nontidal ocean mass, and large-scale hydrological effects. Local hydrological effects contributing significantly to the variation of gravity are beyond the scope of this study. Contributions such as polar motion and length of day are not considered because of the agreement on correction procedures (Hinderer et al., 2015; Van Camp et al., 2017). Details on the uncertainty of some gravity processing procedures such as calibration of relative gravimeters can be found in Meurers (2012) and Van Camp et al. (2016), while the uncertainty of gap fillings and discontinuity corrections are to a certain extend discussed in Hinderer et al. (2002).

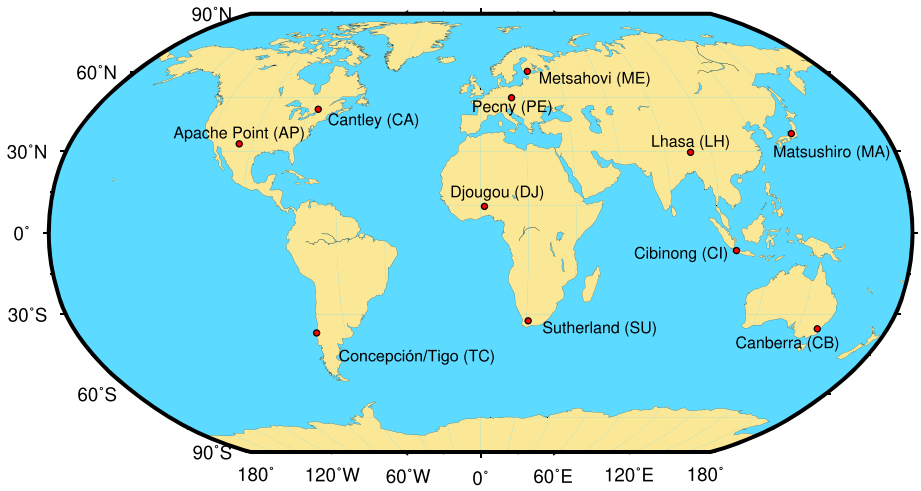

Figure 1. Location of study sites (map created using Wessel et al., 2013).

In order to cover a broad range of conditions, the correction uncertainty is determined for 11 sites worldwide, located in a wide range of latitudes, altitude and in all five major climate zones except of polar according to Kottek et al. (2006) see Figure 1. The sites were selected among the stations of the International Geodynamics and Earth Tide Service (IGETS; Voigt et al., 2016). Several studies provided information on the combined instrumental and environmental noise level at these sites (e.g., Rosat & Hinderer, 2011; Van Camp et al., 2010; Zürn & Widmer, 1995). These studies, however, did not quantify the uncertainty of the corrections that were applied to reduce the environmental noise. A different approach to assess the uncertainty of long-term trends in terrestrial gravity measurements was applied in Van Camp et al. (2016) by considering the impact of water storage estimates of one model or observations (i.e., Gravity Recovery and Climate Experiment) on the trend estimate. Here we present the statistical uncertainty of a set of gravity corrections commonly applied to terrestrial gravity observations by comparing correction models that meet criteria as discussed in the following section. Furthermore, the uncertainty is quantified in the time domain and for temporal changes in the range between 1 hr and 1 year, and for the long-term trend.

2. Data Sets

To simulate realistic scenarios of the gravity correction procedure that apply to any user for any location worldwide, the input models of the geophysical processes to be reduced were selected according to the following criteria: (1) cited and widely recognized model, (2) global spatial coverage, (3) sufficient temporal coverage and resolution, and (4) public availability. The latter criterion includes data sets and software that is available upon request. Criterion (3) limits the choice of models to those starting at least in 2008 and providing data continuously until the present. The starting date was constrained by the availability of actual gravity measurements at the selected sites in the IGETS database. It should be noted, that the actual gravity time series were needed only as input for tidal analysis programs. The data set and the source code used in this study is provided in Mikolaj et al. (2019).

2.1. Tides

Three different software packages were used to estimate the tidal parameters, namely, Baytap(08), ETERNA3.40, and VAV06. All program parameters were set following the recommendation in the respective user manual. This included the tidal wave grouping with the exception of long-periodic waves (up to frequency of 0.7215 cycles per day). The latter were not estimated because of the unknown parameters such as instrumental drift and steps that affect the actual low-frequency variations. The hourly gravity time series of superconducting gravimeters were obtained after downloading from the IGETS database (isdc.gfz-potsdam.de/igets-data-base/, access date 5 March 2018, Boy et al., 2017; Förste et al., 2016; Wziontek et al., 2017). Hourly time series were used for all sites except of Djougou and Cibinong, where these were not available. At these sites, 1-min data were downloaded, calibrated using parameters in the input file header, filtered, and resampled to hourly values. Table S1 in the supporting information shows the time interval entering the tidal analysis at each site. In situ pressure recordings were also used in the tidal anal-

ysis assuming linear relation between gravity and pressure. To remove the unknown low-frequency effects, for example, instrumental drift, the input time series were high-pass filtered prior to the tidal analysis using a finite impulse response filter proposed in the ETERNA3.40 user manual with a cutoff frequency of 0.583 cycles per day. Time series prepared in such manner were then used as input in all three programs using identical tidal potential development and other settings for each site. The three sets of estimated tidal parameter were then used to predict the tidal signal at each site for the common time period starting 1 January 2008 to 31 December 2015 using TSoft (Van Camp & Vauterin, 2005). Thus, the measurements were used only to derive the tidal correction models. The uncertainty was assessed by comparing all available correction models without considering the actual gravity measurements.

2.2. Large-Scale Hydrology

The large-scale hydrological effects from continental water storage variation were computed with seven global hydrological models, namely, four land surface models (CLM, MOS, NOAHv21, and VIC) of the GLDAS model (Rodell et al., 2004), ERA Interim (Dee et al., 2011), MERRA-2 (Gelaro et al., 2017), and NCEP-DOE Reanalysis 2 model (Kanamitsu et al., 2002). The simulated storage variations were converted to gravity effects using the mGlobe toolbox (Mikolaj et al., 2016; download at github.com/emenems/mGlobe, access date 28 February 2018). The large-scale hydrological effects were computed for points with spherical distance greater than 0.1° from the study site. Mass conservation was enforced by applying a uniform layer over the ocean determined by total model mass deficit or surplus as compared to the long-term average. Spurious steps in MERRA-2 and a peak in NCEP-DOE Reanalysis 2 that occurred when enforcing mass conservation were corrected. To suppress the impact of unreliable data of global hydrological models in Antarctica and Greenland, all mass variations in these regions were set to 0. Due to the minimal effect of the temporal resolution on the result (standard deviation below 0.1 nm/s^2), the large-scale hydrological effects were computed for all models with 24-hr time resolution and resampled to hourly resolution afterward.

2.3. Nontidal Ocean Loading

The nontidal ocean loading effects were acquired from EOST Loading Service (Boy et al., 2009) utilizing ECCO-JPL (Fukumori, 2002), ECCO2 (Menemenlis et al., 2008), and TUGOm (Loren & Florent, 2003) models (download at loading.u-strasbg.fr, access date 28 February 2018). In addition, nontidal ocean mass variations of the OMCTv06 model (Dobslaw et al., 2017) were converted to their gravity effect using mGlobe. Identical minimal integration radius of 0.1° from the study site and maximal available model temporal resolution was used in all cases. Linear interpolation was used to resample all time series to hourly resolution. Further details on the effect of the interpolation method on the uncertainty can be found in Mikolaj et al. (2016).

2.4. Global Atmosphere

Empirical or physical approaches can be followed to correct the atmospheric effect on gravity. The empirical approaches called also single admittance utilize in situ air pressure observations converted to a gravity effect by assuming linear relation between these variables. This approach can be further refined by introducing a dependence of the admittance factor on the frequency of the pressure variations (Crossley et al., 1995). As shown in Hinderer et al. (2014), the estimated frequency dependence can be modeled using mass variation output of a physical atmospheric model. The advantage of global atmospheric models is that the computed gravity corrections account also for atmospheric processes occurring far beyond the regional zone. Merriam (1992) showed that single admittance can account for only around 90% of the total atmospheric effect. Hence, the second approach based on modeling of global atmospheric mass variation is analyzed in this study. The disadvantage of global models is the lower temporal resolution compared to in situ pressure, potentially leading to insufficient modeling of processes at shorter periods. This issue is addressed in a separate analysis combining in situ pressure with global models as recommended in the Atmacs model (atmacs.bkg.bund.de/data/, last access date 2 July 2018; Klügel & Wziontek, 2009) and Mikolaj et al. (2016).

The main analysis outlined in section 3 uses following corrections: The EOST service provides global atmospheric effects utilizing European Centre for Medium-Range Weather Forecasts (ECMWF) Operational and ERA Interim models. The latter model was also utilized for an independent computation using mGlobe as, unlike in case of hydrological and oceanic effects, the computation approaches of EOST (2-D) and mGlobe (3-D) differ. Maximal model temporal resolution and the inverted barometer assumption (Egbert & Erofeeva, 2002) was adopted to separate oceanic and atmospheric loading. Linear interpolation was used to resample global corrections to hourly samples that then entered the main uncertainty analysis.

The Atmacs global model was used in addition to the three main models to assess the effect of model spatial resolution on the uncertainty of the correction. The Atmacs model (Klügel & Wziontek, 2009) did not enter the main global analysis because criterion (3) was not met (starting in February 2010 or 2012, see Atmacs global model at atmacs.bkg.bund.de/data/, access date 2 July 2018). The discontinuities of the Atmacs model caused by the change of the input weather forcing data were removed using mean difference to both ECMWF Operational and Interim models.

The separate aforementioned analysis combining in situ pressure with global model was carried out only at 9 of the 11 study sites where global model data overlapped with available in situ pressure observations (see Table S1 in the supporting information). A single admittance factor equal to -3.0 nm/s^2·hPa^{-1} was applied to account for the differences between in situ and model pressure data, called pressure residuals. The choice of the admittance factor affects the uncertainty. A more objective estimation of the admittance factor would require local digital elevation as suggested in Mikolaj et al. (2016). The pressure residuals multiplied by the admittance factor were added to the total correction that was computed using each global atmospheric model.

3. Methods

The uncertainty of the correction models was addressed both in terms of the uncertainty at any point in time (nondifferential mode) and the uncertainty of gravity differences (differential mode). The latter refers to many time domain applications of terrestrial gravimetry where the relative gravity change over a certain time is of major interest to, for example, quantify the change of mass in given interval. These time intervals are hereafter denoted as periods of interest. Furthermore, the uncertainty of the long-term trend was estimated by looking at the slope of a degree 1 polynomial fitted to the deviation between models. The uncertainty of trend estimation in absence of the hydrological correction is discussed in Van Camp et al. (2010, 2016). In the differential mode, each period of interest was separated from the previous one (with shorter period) by an antialiasing zero-phase low-pass filter (see supporting information Figure S1). Due to the need for an efficient number of filter coefficients and the corresponding edge effect, the filtered time series were shortened to 4 years in the differential mode. The differences were then computed for a set of periods of interest ranging from 1 hr up to 1 year. The maximal analyzed period of interest in the analysis combining in situ pressure and global atmospheric model was set to 2 weeks. This limitation reflected the gaps in pressure observations, preventing efficient application of antialiasing filters for long periods. To ensure that the two uncertainty modes can be directly compared, an identical time span was used to compute the uncertainty indicators in the nondifferential mode. This did not not apply to the assessment of the long-term trend where the full 8-year-long time series were used.

In the following, the differences between correction models affecting their uncertainty are denoted as deviations. The deviations were computed at each site in a loop, selecting one reference (i.e., one particular combination of tides, nontidal ocean, hydrology, and atmosphere models taken as the virtual true correction) and one alternative (another combination of the four component models). The alternative was then subtracted from the reference, resulting in a time series of deviations. This loop was repeated for all unique combinations. Combinations leading to zero deviations due to the identical reference and alternative models were not treated as unique. Nonetheless, combinations that result in zeros for individual components (e.g., because the same hydrological model was taken) but nonzero deviations for the full correction were not excluded. This approach allows for selecting combinations where only one component (correction) affects the deviations. Thus, the simplified rule of uncorrelated uncertainty propagation can be applied to estimate the arbitrary combination of components. Combinations leading to deviations with opposite sign were treated as identical, that is, used only once in computing uncertainty indicators. These criteria led to 13,695 combinations at each site considering all four components. As a measure of uncertainty, the RMSE of the deviations was computed. Provided here are the averaged RMSE values over all combinations. Similarly, the mean absolute error (MAE) was computed as an additional uncertainty indicator (results presented in the supporting information). Due to the subtraction of mean value of deviations prior to uncertainty analysis, the RMSE is in essence identical to standard deviation. Only negligible differences were observed between the averaged RMSE and standard deviation caused by the application of filters after mean subtraction in the differential model. Figure 2 summarizes the complete work flow of the global uncertainty analysis applied at each study site.

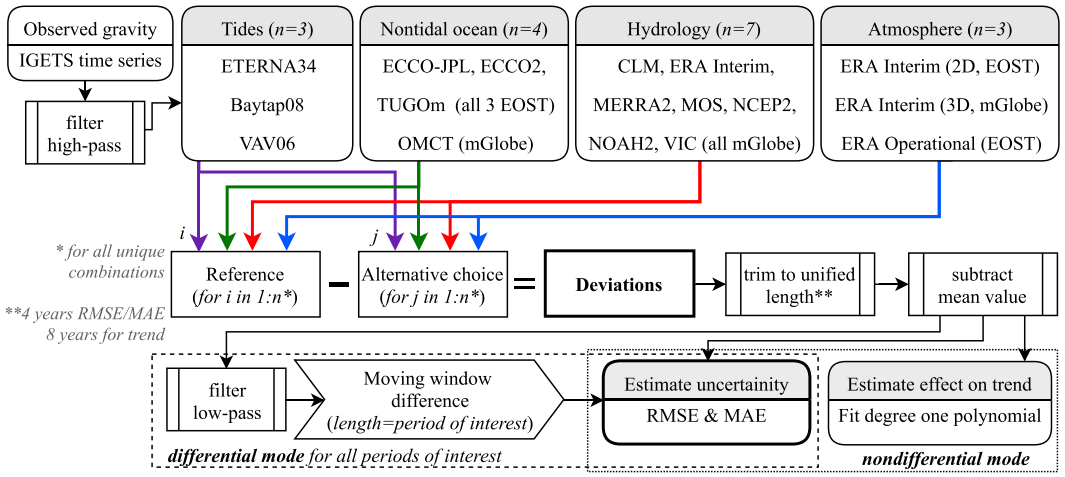

Figure 2. Uncertainty analysis work flow diagram for a single site. EOST = École et Observatoire des Sciences de la Terre; IGETS = International Geodynamics and Earth Tide Service; MAE = mean absolute error; RMSE = root-mean-square error.

To assess the significance of each correction in relation to its amplitude, ratios between the nondifferential RMSE and the peak-to-peak amplitude of the correction were computed. Figure S1 shows the mean amplitudes (half the peak-to-peak range) of each effect in the frequency domain. The time domain amplitude as well as the nondifferential RMSE were computed as a mean over all available models for the respective correction. Any correlation in this study is expressed in terms of the Pearson correlation coefficient.

4. Results

The uncertainties of the correction models in the nondifferential mode are shown in terms of RMSE and for the long-term trend in Figure 3. Results for MAE are shown in Figure S2. The uncertainties of the tidal corrections are the smallest among all components. The mean RMSE value over all sites lies in case of tides below 0.6 nm/s^2. The mean RMSE of nontidal ocean loading effect equals 1.7 nm/s^2, 2.6 nm/s^2 in case of atmosphere, and 3.8 nm/s^2 for large-scale hydrology.

Above-average RMSE values of the nontidal ocean loading effect are anticorrelated with the site distance to the ocean ($r = -0.8$, p value $= 0.003$). The distance of the above-average RMSE sites Cibinong, Matsushiro, Metsahovi and Concepción to the coastline is below 63 km and only 11 km for the latter two sites with the highest uncertainty. Accordingly, the uncertainty of the nontidal ocean loading correction is smallest (below 1 nm/s^2) for sites far from the coastline such as Lhasa and Apache Point. These two sites show the highest uncertainty related to correction of atmospheric effects. This uncertainty is mainly driven by one outlying model, namely, ECMWF Operational (Figure 3e). With the exception of Metsahovi, all sites showing this feature (Apache Point, Lhasa, and Sutherland) are located in high altitude (Table 1). As shown in Mikolaj et al. (2016), the low resolution of ERA Interim leads to insufficient modeling of atmospheric masses close to the actual topography of the Earth. This effect is minimized combining atmospheric model parameters with in situ pressure observations leading to decreased RMSE with the exception of Metsahovi as shown in Figure 5a. Thus, the increased uncertainty at Metsahovi is related to discrepant modeling of atmospheric circulation patterns in the particular region rather than to the topographic effect. Overall, the inclusion of in situ pressure decreases the mean RMSE (computed for all 11 sites) from 2.6 to 1.4 nm/s^2 (computed for nine sites).

The highest contribution to the total uncertainty comes from large-scale hydrology. The mean site-dependent RMSE ranges from 1.4 nm/s^2 (Sutherland) to 6.4 nm/s^2 (Metsahovi) and reaches a maximum of 11.6 nm/s^2 (Djougou) for individual combinations. Similarly to the nontidal ocean loading effect, the uncertainty correlates with the mean peak-to-peak amplitude of the correction ($r = 0.92$, p value $< 10^{-5}$). In addition, the RMSE for large-scale hydrology correlates with latitude ($r = 0.71$, p value $= 0.015$), indicating higher uncertainties in the gravity residuals after hydrology correction in higher latitudes. Due to the major contribution of large-scale hydrology, significant correlation with latitude also translates to total

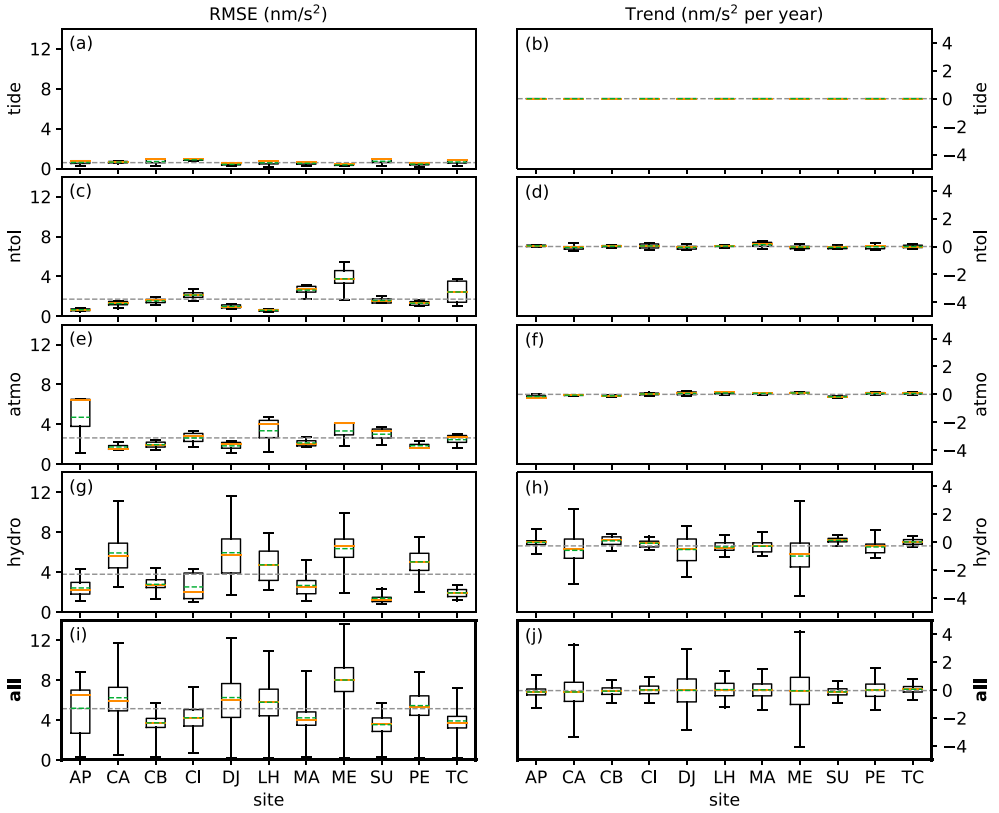

Figure 3. Correction uncertainties in nondifferential mode expressed as RMSE (a, c, e, g, i) and for the long-term trend (b, d, f, h, j) for each study site (columns), for each component (rows), and for the combined uncertainty from all components (lowest row denoted as "all"). Boxes mark the first and third quartiles of all possible combinations; whiskers show the range, median in orange, and mean in green. The gray-line is the mean over all sites. RMSE = root-mean-square error.

uncertainty ($r = 0.78$, p value = 0.005). At 4 out of 11 sites, the maximum RMSE exceeds 10 nm/s^2 with an absolute maximum of 13.7 nm/s^2. The overall mean RMSE over all sites and corrections equals 5.1 nm/s^2.

At none of the sites and for none of the corrections, the ratio between the RMSE and the peak-to-peak amplitude exceeds 30%. Minimal ratios close to 0 were found for tides. On average, the ratio between the RMSE and peak-to-peak amplitude for atmosphere equals 3.0%, 15.9% for nontidal ocean loading, and 18.0% for large-scale hydrology. Hence, the peak-to-peak amplitude of the modeled continental hydrological effect is on average 5 times higher than its uncertainty underlining the significance of the correction despite the increased RMSE. A list of all ratios can be found in Table 2.

The nondifferential results for long-term trends (Figures 3b, 3d, 3f, 3h, and 3j) imply that the deviations between models do not have systematic effects on the trend of corrected gravity. The effect on the trend is on average close to 0 for all sites and corrections. The trend for tides, nontidal oceanic and atmospheric loading is insignificant also when looking at individual model combinations. Only the large-scale hydrology seems to affect the long-term trend for some combinations, with a maximum effect within ±4 nm/s^2·year and the zero line within the first and third quartiles (Figures 3h and 3j).

Uncertainties of correction models in the differential mode are shown in terms of RMSE in Figure 4 and for MAE in Figure S3. For the sake of clarity, these figures present only the mean value over all combinations of the respective correction components at the given periods of interest. Like in the nondifferential mode, tide models play only a minor role for total uncertainty. This applies especially to the uncertainty assessed by comparing the individual tidal models as presented in this study. Actual environmental signals such as evapotranspiration may still interfere with tides, leading to systematic effects that are not reflected in the uncertainty values estimated here. The RMSE reaches a maximum of 1.5 nm/s^2 at 12 hr in Cibinong. For the same period, the minimum RMSE lies at 0.6 nm/s^2 in Djougou. The mean over all

Table 1
Study Sites

Site Name	ID	λ (°)	ϕ (°)	H (m)	Climate[a]	Position Coast[b]
Apache Point	AP	−105.82	32.78	2788	Cfb	706
Cantley	CA	−75.8	45.59	269	Dfb	108
Canberra	CB	149.0	−35.32	763	Cfb	116
Cibinong	CI	106.85	−6.49	138	Af	43
Djougou	DJ	1.61	9.74	483	Aw	385
Lhasa	LH	91.04	29.65	3600	BSk	670
Matsushiro	MA	138.20	36.54	451	Cfa	63
Metsahovi	ME	24.10	60.22	56	Dfb	11
Pecny	PE	14.79	49.91	535	Cfb	410
Sutherland	SU	20.81	−32.38	1791	BSk	219
Concepción	TC	−73.03	−36.84	156	Csb	11

[a] Derived after Rubel et al. (2017). [b] Distance (km) to coastline computed using Natural Earth website (naturalearthdata.com).

worldwide sites equals 1.1 nm/s^2 (Figures 6 and S4). Tidal waves with a period larger than 33 hr were not considered here because of the unknown instrumental effects interfering with the long-periodic tidal waves (RMSE equals 0 in Figure 4a). The nontidal ocean loading correction affects the uncertainties of gravity changes across all periods of interest. The RMSE does not exceed 2 nm/s^2 for most sites and periods of interest. This value is exceeded only at three sites close to the coastline (Matsushiro, Metsahovi, and Concepción). The mean RMSE reaches a maximum of 1.6 nm/s^2 at 48-hr period. The uncertainty of the global atmospheric correction on gravity in the differential mode shows several local maxima. These maxima highlight the different dominant atmospheric processes at the different sites. At Cibining, Djougou, Sutherland, and Lhasa, the atmospheric mass transport is driven mainly by solar atmospheric tides S2 and S1. Discrepancies in modeling approaches of these phenomena by different atmospheric models leads to increased uncertainty. In turn, clear maximum RMSE of 3.7, 2.6, and 1.8 nm/s^2 is found at 6 hr for the former three sites and 3.2 nm/s^2 at 12 hr in Lhasa. The maximum uncertainty lies at the half of the dominant period because deviations of gravity changes in time are assessed in the differential mode. Therefore, a deviation with a clear 24-hr period will lead to high uncertainty for 12-hr differences, computed in the

Table 2
Ratio of RMSE and Peak-to-Peak Amplitude of the Corrections (Rounded to One Decimal Place)

Site ID	Tide (‰)	ntol[a](%)	atmo[b](%)	hydro[c](%)
AP	0.2	14.7	5.2	17.2
CA	0.2	17.6	0.9	14.4
CB	0.2	14.0	1.2	17.3
CI	0.3	12.9	8.2	17.5
DJ	0.1	15.6	5.3	18.0
LH	0.2	17.1	3.9	22.5
MA	0.2	17.2	1.3	26.8
ME	0.2	16.2	1.2	18.2
PE	0.2	15.6	1.0	13.6
SU	0.2	13.3	3.0	20.4
TC	0.2	20.6	2.0	11.6
Mean[d]	0.2	15.9	3.0	18.0

[a]Nontidal ocean loading. [b]Atmosphere. [c]Continental hydrology. [d]Average over all sites.

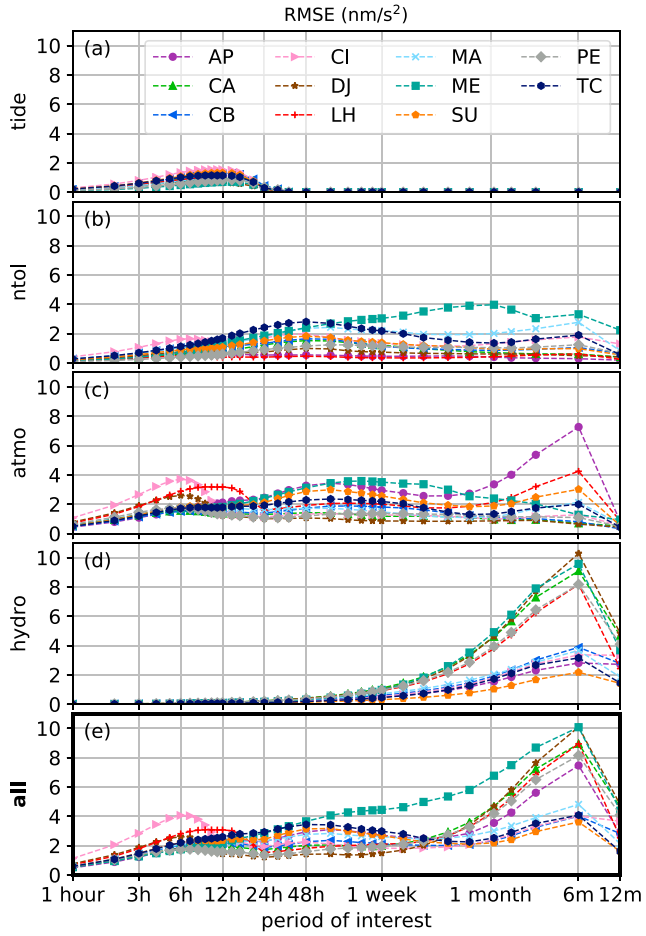

Figure 4. Correction uncertainties in differential mode, for each study site and each component (a–d) and for the combined uncertainty from all components (e). *X* axis is in logarithmic scale. RMSE = root-mean-square error.

worst case from the difference at the maximum and minimum of a periodic oscillation. An identical phenomenon is observed for large-scale hydrological corrections with a dominant 12-month period. For the remaining sites, local maximum can be found between 6 hr to 5 days ranging from 1.7 nm/s^2 (Pecny) to 3.6 nm/s^2 (Metsahovi) and a mean maximum value over all sites of 2.1 nm/s^2 around 72 hr (Figure 6). The combination of a global atmospheric model with in situ pressure data reduces the uncertainty at all site and for all analyzed periods of interest with the exception of Metsahovi at periods of around 1 week (see Figure 5b). On average, the RMSE in the differential mode is reduced after inclusion of in situ pressure by a factor of 2.4. The uncertainty related to the correction of the large-scale hydrological effect shows a distinct maximum at 6 months and exceeds 10 nm/s^2 at one site (Djougou). The mean maximum RMSE for large-scale hydrology over all sites equals 5.9 nm/s^2. The total uncertainty in the differential model over all sites and corrections (Figure 6) is dominated by the large-scale hydrology with maximum of 6.7 nm/s^2 at the 6-month period. The total RMSE exceeds 2 nm/s^2 at all periods longer then 5 hr. The minimum uncertainty of 0.6 nm/s^2 is found for hourly gravity variations owing especially to the atmospheric correction. This value is reduced to 0.2 nm/s^2 if the correction is computed by combining the in situ pressure data with the global model.

5. Discussion

The comparatively high uncertainty of the atmospheric correction is mainly caused by the deviation between ERA Operational and Interim in high-altitude regions. The prioritization of high-resolution models one may argue for, however, does not necessarily lead to more trustful results. The uncertainty in terms of RMSE is not reduced when replacing the correction based on ERA Interim model by the Atmacs correction, which makes

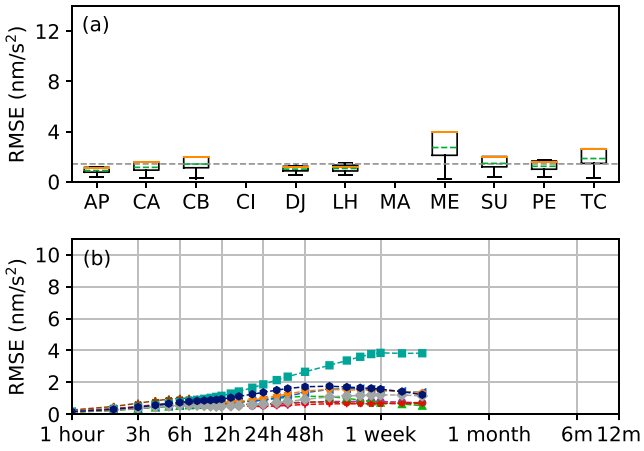

Figure 5. Nondifferential (a) and differential mode (b) RMSE of the atmospheric correction computed combining in situ pressure and global model at selected study site. See Figures 3 and 4 for legend and other details describing the (a) and (b) plots, respectively.

use of a high-resolution weather model similar to ERA Operational (see Figure S5 in supporting information). This example underlines the inherent difficulty to assess which correction model might performance best at a certain study site. Unless all corrections are taken into consideration, criteria such as reduction of residuals used in similar studies (e.g., Xu, 2017) cannot by reasonably employed in case of terrestrial gravity measurements. This can be illustrated for underground gravity sites where the local hydrology interferes with large-scale signals and any correction of large-scale effects leads to increased variability of residuals regardless of the precision of the used model (Longuevergne et al., 2009). Different criteria for model performance, such as choice of model closest to overall mean, are also problematic, especially because of systematic errors. Any model-specific deficits, for example, missing groundwater compartment in hydrological models, the tidal wave grouping, nonconsideration of long-periodic tides, choice of pressure admittance, or quality of gravity series preprocessing (gap filling, discontinuity correction, etc.), are not reflected in the uncertainty indicators. Furthermore, the estimated uncertainties reflect the dispersion among the models used here within the studied period. Any new development of correction models may lead to new estimates. The dispersion of the atmospheric corrections is significantly reduced when combining global model with in situ pressure. Such an approach tends to diminish the model discrepancies toward a given reference (in situ pressure) without knowledge of the true total atmospheric gravity effect. Thus, the results do not describe the absolute precision of gravity residuals but rather the precision of corrections assessed using state-of-the-art global models available to users worldwide.

Uncertainty assessed in this manner is limited by the rather small number of study sites. The low number of IGETS sites needed for the tidal analysis, especially in latitude range ±20°, manifests itself in clustering of the RMSE due to large-scale hydrology correction into the two groups prominent in Figure 4d. Nevertheless, the study sites cover an extended latitude and altitude range, distance to coastline, all continents and climate zones with the exception of polar region. Hence, the extreme values are well represented by the characteristic sites of the respective region. The use of regional models that assimilate local observations might be advisable in certain regions, for example, at Metsahovi with distinct nontidal and atmospheric effects in the Baltic Sea. These models should, however, be combined with large-scale models to account for global mass transport processes, especially when using high-precision superconducting gravimeters capable of detecting such phenomena.

Depending on the field of research, the uncertainties in gravity units (nm/s^2) obtained here can be converted to units of interest, such as kilograms of water or millimeters of land uplift, using gravity modeling, or they can be directly compared to the expected signal amplitudes of interest, as listed in the review article of Van Camp et al. (2017). Such comparisons show that the uncertainty related to gravity corrections does not hinder the resolution of substantial effects of interest in most of the research fields including hydrology, volcanology, reservoir monitoring, or local subsidence, all exceeding tens of nanometers per square second. However, subtle effects in the order of few nanometers per square second, that is, on the lower part of the

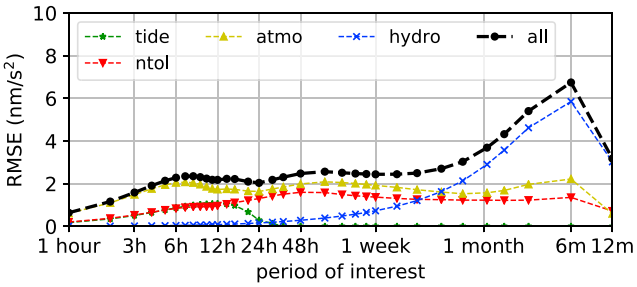

Figure 6. Correction uncertainties in differential mode, computed as mean over all study sites for each component (combined contribution denoted as "all") using global atmospheric correction without in situ pressure. *X* axis is in logarithmic scale. RMSE = root-mean-square error.

expected signature level, will be difficult to be resolved. This is because of the uncertainty of the gravity corrections adding to the instrumental precision (see section 1). Therefore, a meaningful use of gravimeters in studies focusing on subtle changes requires employment of advanced processing techniques such as stacking, filtering, or use of additional constrains suppressing random errors, for example, as employed in Güntner et al. (2017) and Van Camp et al. (2016).

6. Conclusions

The uncertainty of terrestrial gravity correction models for tides, atmospheric, large-scale hydrological, and nontidal ocean loading effects was assessed using a large set of available global models. The presented values can be used to estimate the correction-induced uncertainty in cases where users apply one or all of the mentioned corrections in order to reduce the environmental effect on observed gravity. The obtained RMSE at 11 sites worldwide equals 5.1 nm/s^2. This value gives the average uncertainty that affects gravity residuals without taking local corrections of hydrology or in situ pressure into account. The estimate does not include other random and systematic errors such as instrumental effects or near-field noise. The uncertainty varies significantly with location and is correlated to geographical latitude owing especially to the large-scale hydrological effects. Depending on the study site, the uncertainty can range from 3.5 nm/s^2 up to a maximum of 8.0 nm/s^2. A high negative correlation has also been found between the site distance to the ocean and the uncertainty due to nontidal ocean loading correction. The total correction uncertainty is mainly driven by the deviations between large-scale hydrological models with 3.8 nm/s^2, as compared to 2.6, 1.7, and 0.6 nm/s^2 for global atmospheric, nontidal ocean loading and tides correction, respectively. For many studies focused on quantifying mass changes over time, the uncertainty of gravity differences in time are of interest. We have studied differences between 1 hr up to 12 months and found that the hourly differences show the lowest uncertainty in terms of RMSE equal to 0.6 nm/s^2. The analysis using global models shows that the uncertainty of differences longer than 5 hr exceeds on average 2 nm/s^2 and reach a maximum of 6.7 nm/s^2 for intervals of 6 months. This implies that observing seasonal mass variations by terrestrial gravimetry is burdened with highest correction uncertainty. The overall and the atmospheric correction uncertainty are reduced to 4.4 and 1.4 nm/s^2, respectively, if global models are combined with actual in situ pressure observations. Such approach also affects the uncertainty of gravity differences, reducing the RMSE to 0.2 nm/s^2 for hourly estimates, for instance.

Small to negligible systematic uncertainties on the long-term trend were found. The ratio between the amplitude of the correction and the RMSE (equivalent to standard deviation σ) shows that the peak-to-peak amplitudes are in most cases at least 5 times higher than the uncertainty. This indicates that the corrections should be, from statistical point of view, taken into consideration despite their uncertainty. Overall, the results of this study demonstrate that substantial mass changes associated with a diversity of geophysical processes can be confidently resolved by terrestrial gravimetry even though necessary signal corrections impose nonnegligible uncertainties. Thus, any direct resolution of subtle gravity changes in the order of few nanometers per square second might be hindered by the total uncertainty composed of the instrumental and correction precision. Consequently, advancing to higher-precision gravimetry application is not only subject of further technological development of the gravimeters themselves but also of improving the representation of mass transport processes in various components of the Earth system and at various spatial scales.

Acknowledgments
Yoshiaki Tamura (NAOJ), Duncan Agnew (UCSD), Jose Arnoso Sampedro (CSIC-UCM), and the IGETS service are acknowledged for developing and providing Baytap(08), VAV06, and ETERNA programs. We also thank Hartmut Wziontek (BKG, Leipzig) and Daniel Beiter (GFZ Potsdam) for fruitful discussions on various topics related to this publication. Two anonymous reviewers are gratefully acknowledged for their constructive comments. We are deeply indebted to the Julia, Octave, and R developer community. Observed gravity time series and OMCT data used in this study were obtained from the Information System and Data Center for geoscientific data (ISDC) at GFZ Potsdam. The EOST modeled gravity effect time series were obtained from EOST Loading Service. The GLDAS and MERRA data used in this study were acquired as part of the mission of NASA's Earth Science Division and archived and distributed by the Goddard Earth Sciences (GES) Data and Information Services Center (DISC). The ERA-Interim data used in this study was obtained from the ECMWF data server. The NCEP Reanalysis data were provided by the NOAA/OAR/ESRL PSD, Boulder, Colorado, USA, via their web server. A part of this study was carried out within the "Hydrological and oceanic signals in geodetic observations at the Argentine-German Geodetic Observatory (HOSGO)" project (01DN16019) funded jointly by Bundesministerium für Bildung und Forschung (BMBF) and Consejo Nacional de Investigaciones Cientficas y Técnicas (CONICET). Repository containing processing scripts and outputs, as well as an explanatory read-me file with all instructions for reproducing the results presented in this study are available via GFZ Data Services (Mikolaj et al., 2019).

References

Arnoso, J., Benavent, M., Bos, M., Montesinos, F., & Vieira, R. (2011). Verifying the body tide at the Canary Islands using tidal gravimetry observations. *Journal of Geodynamics*, *51*(5), 358–365. https://doi.org/10.1016/j.jog.2010.10.004

Boy, J. P., & Hinderer, J. (2006). Study of the seasonal gravity signal in superconducting gravimeter data. *Journal of Geodynamics*, *41*(1–3), 227–233. https://doi.org/10.1016/j.jog.2005.08.035

Boy, J. P., Longuevergne, L., Boudin, F., Jacob, T., Lyard, F., Llubes, M., & Esnoult, M. F. (2009). Modelling atmospheric and induced non-tidal oceanic loading contributions to surface gravity and tilt measurements. *Journal of Geodynamics*, *48*(3–5), 182–188. https://doi.org/10.1016/j.jog.2009.09.022

Boy, J. P., Rosat, S., Hinderer, J., & Littel, F. (2017). *Superconducting gravimeter data from Djougou - Level 1*. https://doi.org/10.5880/igets.dj.l1.001

Carbone, D., Poland, M. P., Diament, M., & Greco, F. (2017). The added value of time-variable microgravimetry to the understanding of how volcanoes work. *Earth-Science Reviews*, *169*, 146–179. https://doi.org/10.1016/j.earscirev.2017.04.014

Creutzfeldt, B., Troch, P. A., Güntner, A., Ferré, T. P. A., Graeff, T., & Merz, B. (2013). Storage-discharge relationships at different catchment scales based on local high-precision gravimetry. *Hydrological Processes*, *28*(3), 1465–1475. https://doi.org/10.1002/hyp.9689

Crossley, D., Hinderer, J., & Riccardi, U. (2013). The measurement of surface gravity. *Reports on Progress in Physics*, *76*(4), 46101.

Crossley, D. J., Jensen, O. G., & Hinderer, J. (1995). Effective barometric admittance and gravity residuals. *Physics of the Earth and Planetary Interiors*, *90*(3), 221–241. https://doi.org/10.1016/0031-9201(95)05086-Q

Dee, D. P., Uppala, S. M., Simmons, A. J., Berrisford, P., Poli, P., Kobayashi, S., & Vitart, F. (2011). The ERA-Interim reanalysis: Configuration and performance of the data assimilation system. *Quarterly Journal of the Royal Meteorological Society*, *137*(656), 553–597. https://doi.org/10.1002/qj.828

Dobslaw, H., Bergmann-Wolf, I., Dill, R., Poropat, L., Thomas, M., Dahle, C., & Flechtner, F. (2017). A new high-resolution model of non-tidal atmosphere and ocean mass variability for de-aliasing of satellite gravity observations: AOD1B RL06. *Geophysical Journal International*, *211*(1), 263–269. https://doi.org/10.1093/gji/ggx302

Egbert, G. D., & Erofeeva, S. Y. (2002). Efficient inverse modeling of barotropic ocean tides. *Journal of Atmospheric and Oceanic Technology*, *19*(2), 183–204. https://doi.org/10.1175/1520-0426(2002)019<0183:EIMOBO>2.0.CO;2

Förste, C., Voigt, C., Abe, M., Kroner, C., Neumeyer, J., Pflug, H., & Fourie, P. (2016). *Superconducting gravimeter data from Sutherland - Level 1* https://doi.org/10.5880/igets.su.l1.001

Fukumori, I. (2002). A partitioned Kalman filter and smoother. *Monthly Weather Review*, *130*(5), 1370–1383. https://doi.org/10.1175/1520-0493(2002)130<1370:APKFAS>2.0.CO;2

Gelaro, R., McCarty, W., Suárez, M. J., Todling, R., Molod, A., Takacs, L., & Zhao, B. (2017). The Modern-Era Retrospective Analysis for Research and Applications, Version 2 (MERRA-2). *Journal of Climate*, *30*(14), 5419–5454. https://doi.org/10.1175/JCLI-D-16-0758.1

Gillot, P., Francis, O., Landragin, A., Dos Santos, F. P., & Merlet, S. (2014). Stability comparison of two absolute gravimeters: Optical versus atomic interferometers. *Metrologia*, *51*(5), L15–L17. https://doi.org/10.1088/0026-1394/51/5/l15

Güntner, A., Reich, M., Mikolaj, M., Creutzfeldt, B., Schroeder, S., & Wziontek, H. (2017). Landscape-scale water balance monitoring with an iGrav superconducting gravimeter in a field enclosure. *Hydrology and Earth System Sciences*, *21*(6), 3167–3182. https://doi.org/10.5194/hess-21-3167-2017

Hector, B., Hinderer, J., Séguis, L., Boy, J. P., Calvo, M., Descloitres, M., & Riccardi, U. (2014). Hydro-gravimetry in West-Africa: First results from the Djougou (Benin) superconducting gravimeter. *Journal of Geodynamics*, *80*, 34–49. https://doi.org/10.1016/j.jog.2014.04.003

Hector, B., Séguis, L., Hinderer, J., Cohard, J. M., Wubda, M., Descloitres, M., & Boy, J. P. (2015). Water storage changes as a marker for base flow generation processes in a tropical humid basement catchment (Benin): Insights from hybrid gravimetry. *Water Resources Research*, *51*, 8331–8361. https://doi.org/10.1002/2014WR015773

Hinderer, J., Crossley, D., & Warburton, R. J. (2015). 3.04—Gravimetric methods—Superconducting gravity meters. In G. Schubert (Ed.), *Treatise on geophysics* (Vol. 3, pp. 59–115). Amsterdam, Netherlands: Elsevier. https://doi.org/10.1016/B978-0-444-53802-4.00062-2

Hinderer, J., Hector, B., Boy, J. P., Riccardi, U., Rosat, S., Calvo, M., & Littel, F. (2014). A search for atmospheric effects on gravity at different time and space scales. *Journal of Geodynamics*, *80*, 50–57. https://doi.org/10.1016/j.jog.2014.02.001

Hinderer, J., Rosat, S., Crossley, D., Amalvict, M., Boy, J. P., & Gegout, P. (2002). Influence of different processing methods on the retrieval of gravity signals from GGP data. *Bulletin d'Information des Marées Terrestres*, *135*, 10,653–10,668.

Imanishi, Y., Sato, T., Higashi, T., Sun, W., & Okubo, S. (2004). A network of superconducting gravimeters detects submicrogal coseismic gravity changes. *Science*, *306*(5695), 476–478. https://doi.org/10.1126/science.1101875

Joint Committee for Guides in Metrology (2008). Joint Committee for Guides in Metrology: Evaluation of measurement data—Guide to the expression of uncertainty in measurement. Bureau International des Poids et Mesures.

Kanamitsu, M., Ebisuzaki, W., Woollen, J., Yang, S. K., Hnilo, J. J., Fiorino, M., & Potter, G. L. (2002). NCEP-DOE AMIP-II Reanalysis (R-2). *Bulletin of the American Meteorological Society*, *83*(11), 1631–1644. https://doi.org/10.1175/BAMS-83-11-1631

Kao, R., Kabirzadeh, H., Kim, J. W., Neumeyer, J., & Sideris, M. G. (2014). Detecting small gravity change in field measurement: Simulations and experiments of the superconducting gravimeter—iGrav. *Journal of Geophysics and Engineering*, *11*(4), 1–11.

Klügel, T., & Wziontek, H. (2009). Correcting gravimeters and tiltmeters for atmospheric mass attraction using operational weather models. *Journal of Geodynamics*, *48*(3–5), 204–210. https://doi.org/10.1016/j.jog.2009.09.010

Kottek, M., Grieser, J., Beck, C., Rudolf, B., & Rubel, F. (2006). World map of the Köppen-Geiger climate classification updated. *Meteorologische Zeitschrift*, *15*(3), 259–263. https://doi.org/10.1127/0941-2948/2006/0130

Longuevergne, L., Boy, J. P., Florsch, N., Viville, D., Ferhat, G., Ulrich, P., & Hinderer, J. (2009). Local and global hydrological contributions to gravity variations observed in Strasbourg. *Journal of Geodynamics*, *48*(3–5), 189–194. https://doi.org/10.1016/j.jog.2009.09.008

Loren, C., & Florent, L. (2003). Modeling the barotropic response of the global ocean to atmospheric wind and pressure forcing-comparisons with observations. *Geophysical Research Letters*, *30*(6), 1275. https://doi.org/10.1029/2002GL016473

Menemenlis, D., Campin, J., Heimbach, P., Hill, C., Lee, T., Nguyen, A., & Zhang, H. (2008). ECCO2: High resolution global ocean and sea ice data synthesis. *Mercator Ocean Quarterly Newsletter*, *31*, 13–21.

Ménoret, V., Vermeulen, P., Moigne, N. L., Bonvalot, S., Bouyer, P., Landragin, A., & Desruelle, B. (2018). Gravity measurements below $10^{-9}g$ with a transportable absolute quantum gravimeter. *Scientific Reports*, *8*(1), 12300. https://doi.org/10.1038/s41598-018-30608-1

Merriam, J. B. (1992). Atmospheric pressure and gravity. *Geophysical Journal International*, *109*(3), 488–500. https://doi.org/10.1111/j.1365-246X.1992.tb00112.x

Meurers, B. (2012). Superconducting gravimeter calibration by coLocated gravity observations: Results from GWR C025. *International Journal of Geophysics*, *2012*, 1–12. https://doi.org/10.1155/2012/954271

Meurers, B., Van Camp, M., Francis, O., & Pálinkáš, V. (2016). Temporal variation of tidal parameters in superconducting gravimeter time-series. *Geophysical Journal International*, *205*(1), 284–300. https://doi.org/10.1093/gji/ggw017

Middlemiss, R. P., Samarelli, A., Paul, D. J., Hough, J., Rowan, S., & Hammond, G. D. (2016). Measurement of the Earth tides with a MEMS gravimeter. *Nature*, *531*(7596), 614–617. https://doi.org/10.1038/nature17397

Mikolaj, M., Meurers, B., & Güntner, A. (2016). Modelling of global mass effects in hydrology, atmosphere and oceans on surface gravity. *Computers & Geosciences*, *93*, 12–20. https://doi.org/10.1016/j.cageo.2016.04.014

Mikolaj, M., Meurers, B., & Mojzeš, M. (2015). The reduction of hydrology-induced gravity variations at sites with insufficient hydrological instrumentation. *Studia Geophysica et Geodaetica*, *59*(3), 424–437. https://doi.org/10.1007/s11200-014-0232-8

Mikolaj, M., Reich, M., & Güntner, A. (2019). Supporting information to: Resolving geophysical signals by terrestrial gravimetry: A time domain assessment of the correction-induced uncertainty. *GFZ Data Services*. https://doi.org/10.5880/GFZ.4.4.2019.001

Ophaug, V., Breili, K., Gerlach, C., Gjevestad, J. G. O., Lysaker, D. I., Omang, O. C. D., & Pettersen, B. R. (2016). Absolute gravity observations in Norway (1993–2014) for glacial isostatic adjustment studies: The influence of gravitational loading effects on secular gravity trends. *Journal of Geodynamics*, *102*, 83–94. https://doi.org/10.1016/j.jog.2016.09.001

Plag, H. P., & Pearlman, M. (2009). *Global geodetic observing system*. Berlin: Springer-Verlag.

Poland, M. P., & Carbone, D. (2016). Insights into shallow magmatic processes at Kilauea Volcano, Hawaii, from a multiyear continuous gravity time series. *Journal of Geophysical Research: Solid Earth*, *121*, 5477–5492. https://doi.org/10.1002/2016JB013057

Rodell, M., Houser, P. R., Jambor, U., Gottschalck, J., Mitchell, K., Meng, C. J., & Toll, D. (2004). The Global Land Data Assimilation System. *Bulletin of the American Meteorological Society*, *85*(3), 381–394. https://doi.org/10.1175/BAMS-85-3-381

Rosat, S., & Hinderer, J. (2011). Noise levels of superconducting gravimeters: Updated comparison and time stability. *Bulletin of the Seismological Society of America*, *101*(3), 1233. https://doi.org/10.1785/0120100217

Rosat, S., & Hinderer, J. (2018). Limits of detection of gravimetric signals on Earth. *Scientific Reports*, *8*, 15324. https://doi.org/10.1038/s41598-018-33717-z

Rubel, F., Brugger, K., Haslinger, K., & Auer, I. (2017). The climate of the European Alps: Shift of very high resolution Köppen-Geiger climate zones 1800–2100. *Meteorologische Zeitschrift*, *26*(2), 115–125. https://doi.org/10.1127/metz/2016/0816

Stock, M. (2013). Watt balance experiments for the determination of the Planck constant and the redefinition of the kilogram. *Metrologia*, *50*(1), R1.

Sugihara, M., Nishi, Y., Ikeda, H., Nawa, K., & Ishido, T. (2017). Monitoring CO_2 injection at the Tomakomai Field using high-sensitivity continuous gravimetry. *Energy Procedia*, *114*, 4020–4027. https://doi.org/10.1016/j.egypro.2017.03.1542

Tamura, Y., Sato, T., Ooe, M., & Ishiguro, M. (1991). A procedure for tidal analysis with a Bayesian information criterion. *Geophysical Journal International*, *104*(3), 507–516. https://doi.org/10.1111/j.1365-246X.1991.tb05697.x

Tanaka, T., Miyajima, R., Asai, H., Horiuchi, Y., Kumada, K., Asai, Y., & Ishii, H. (2013). Hydrological gravity response detection using a gPhone below- and aboveground. *Earth, Planets and Space*, *65*(2), 59–66. https://doi.org/10.5047/eps.2012.06.012

Vallée, M., Ampuero, J. P., Juhel, K., Bernard, P., Montagner, J. P., & Barsuglia, M. (2017). Observations and modeling of the elastogravity signals preceding direct seismic waves. *Science*, *358*(6367), 1164–1168. https://doi.org/10.1126/science.aao0746

Van Camp, M., de Viron, O., & Avouac, J. (2016). Separating climate-induced mass transfers and instrumental effects from tectonic signal in repeated absolute gravity measurements. *Geophysical Research Letters*, *43*, 4313–4320. https://doi.org/10.1002/2016GL068648

Van Camp, M., de Viron, O., Pajot-Métivier, G., Casenave, F., Watlet, A., Dassargues, A., & Vanclooster, M. (2016). Direct measurement of evapotranspiration from a forest using a superconducting gravimeter. *Geophysical Research Letters*, *43*, 10,225–10,231. https://doi.org/10.1002/2016GL070534

Van Camp, M., de Viron, O., Scherneck, H. G., Hinzen, K. G., Williams, S. D. P., Lecocq, T., & Camelbeeck, T. (2011). Repeated absolute gravity measurements for monitoring slow intraplate vertical deformation in western Europe. *Journal of Geophysical Research*, *116*, B08402. https://doi.org/10.1029/2010JB008174

Van Camp, M., de Viron, O., Watlet, A., Meurers, B., & Francis, O. C. C. (2017). Geophysics from terrestrial time-variable gravity measurements. *Reviews of Geophysics*, *55*, 938–992. https://doi.org/10.1002/2017RG000566

Van Camp, M., Métivier, L., de Viron, O., Meurers, B., & Williams, S. D. P. (2010). Characterizing long-time scale hydrological effects on gravity for improved distinction of tectonic signals. *Journal of Geophysical Research*, *115*, B07407. https://doi.org/10.1029/2009JB006615

Van Camp, M., Meurers, B., Viron, O., & Forbriger, T. (2016). Optimized strategy for the calibration of superconducting gravimeters at the one per mille level. *Journal of Geodesy*, *90*(1), 91–99. https://doi.org/10.1007/s00190-015-0856-7

Van Camp, M., & Vauterin, P. (2005). Tsoft: Graphical and interactive software for the analysis of time series and Earth tides. *Computers & Geosciences*, *31*(5), 631–640. https://doi.org/10.1016/j.cageo.2004.11.015

Van Camp, M., Williams, S. D. P., & Francis, O. (2005). Uncertainty of absolute gravity measurements. *Journal of Geophysical Research*, *110*, B05406. https://doi.org/10.1029/2004JB003497

van Dam, T., Francis, O., Wahr, J., Khan, S. A., Bevis, M., & van den Broeke, M. R. (2017). Using GPS and absolute gravity observations to separate the effects of present-day and Pleistocene ice-mass changes in South East Greenland. *Earth and Planetary Science Letters*, *459*, 127–135. https://doi.org/10.1016/j.epsl.2016.11.014

Venedikov, A. P., Arnoso, J., & Vieira, R. (2005). New version of program VAV for tidal data processing. *Computers & Geosciences*, *31*(5), 667–669. https://doi.org/10.1016/j.cageo.2004.12.001

Voigt, C., Förste, C., Wziontek, H., Crossley, D., Meurers, B., Pálinkáš, V., & Sun, H. (2016). Report on the data base of the International Geodynamics and Earth Tide Service (IGETS). https://doi.org/10.2312/GFZ.b103-16087

Wenzel, H. G. (1996). The nanogal software: Earth tide data processing package ETERNA 3.30. *Bulletin d'Informations Marées Terrestres*, *124*, 9425–9439.

Wessel, P., Smith, W. H. F., Scharroo, R., Luis, J., & Wobbe, F. (2013). Generic mapping tools: Improved version released. *Eos, Transactions American Geophysical Union*, *94*(45), 409–410. https://doi.org/10.1002/2013EO450001

Wziontek, H., Wolf, P., Böer, A., Hase, H., Nowak, I., Richter, B., & Wilmes, H. (2017). https://doi.org/10.5880/igets.tc.l1.001

Xu, C. (2017). Evaluating mass loading products by comparison to GPS array daily solutions. *Geophysical Journal International*, *208*(1), 24–35. https://doi.org/10.1093/gji/ggw385

Zürn, W., & Widmer, R. (1995). On noise reduction in vertical seismic records below 2 mHz using local barometric pressure. *Geophysical Research Letters*, *22*(24), 3537–3540. https://doi.org/10.1029/95GL03369